FULL PAPER

ADVANCED
INTELLIGENT
SYSTEMS
Open Access

www.advintellsyst.com

Liquid Metal-Based Strain Sensor with Ultralow Detection Limit for Human–Machine Interface Applications

Yuanzhao Wu, Youlin Zhou, Waqas Asghar, Yiwei Liu,* Fali Li, Dandan Sun, Chao Hu, Zhenguang Wu, Jie Shang, Zhe Yu, Run-Wei Li,* and Huali Yang

Flexible strain sensors play vital role in human–machine interaction. Despite their vast development, a strain sensor having broad strain sensing range, ultralow detection limit, and negligible hysteresis still remains a challenge. Herein, a liquid metal (LM)-based stretchable resistive strain sensor, prepared by selective wetting and transferring process to attain improved compatibility between LM and polydimethylsiloxane substrate, is reported. This sensor exhibits broad strain sensing range (105%), with ultralow detection limit (0.05%), minimal hysteresis, fast response time (58 ms), and excellent repeatability. When practically demonstrated, this sensor successfully monitored various human activities, such as blink motion monitoring, voice intensity differentiation, heartbeat and wrist pulse monitoring. Moreover, when the current sensor is used in the form of smart kneecap and smart glove, it efficiently detected various human gestures, which confirms its great application potential in the fields of human health and motion monitoring, human–machine interface, and virtual reality applications.

1. Introduction

Human–machine interaction (HMI) enables two-way information transfer between humans and machines (such as computers or robots).[1] Conventional rigid HMIs are widely used in various applications, such as rehabilitation robots, motion gesture monitoring, and biological health monitoring. However, their rigid nature leads to discomfort and unstable signal problem during the motion of human body. Alternatively, soft HMIs provide all the sensing functions of conventional rigid HMIs but with the ability of being stretched, compressed, twisted, bent, and deformed into arbitrary shapes.[2] Nowadays, soft HMIs

are realizing such innovative applications that are impossible for rigid HMIs.

Flexible strain sensors are important component of soft HMI systems.[3] To date, significant efforts are made to develop flexible strain sensors with ultralow detection limit and broad sensing range. Generally, the performance of a strain sensor is improved by choosing stretchable polymers or by designing novel sensing structures.[3–5] Bao et al. have reported carbon nanotube (CNT)-based spiral-structured stretchable strain sensor that can accommodate stretching strain up to 150%.[6] In contrast, a variety of structures are designed to enhance the performance of strain sensors. For instance, Kang et al. have developed strain sensors by generating cracks in the platinum (Pt) film, which demonstrated the detection limit of 0.1% and a gauge factor of over 2000, within 0–2% strain range.[7] Peng et al. manufactured a strain sensor by depositing CNTs on spiral-shaped polypropylene fiber and achieved wide sensing range of 200% strain with ultralow detection limit of 0.01%.[8] Despite these advancements, a strain sensor having precise displacement–resistance response with high resolution, ultralow detection limit, and broad sensing range still remains a challenge.

Gallium-based LM alloys are considered highly suitable material for stretchable strain sensors because of their capability of retaining high electrical conductivity even under extreme stretch condition.[9,10] These LMs exhibit low viscosity and fluidic nature, which enables LM to follow the deformation path of soft

Dr. Y. Wu, Y. Zhou, W. Asghar, Prof. Y. Liu, F. Li, D. Sun, C. Hu, Z. Wu, Prof. J. Shang, Z. Yu, Prof. R.-W. Li, Dr. H. Yang
CAS Key Laboratory of Magnetic Materials and Devices
Ningbo Institute of Materials Technology and Engineering
Chinese Academy of Sciences
Ningbo 315201, P. R. China
E-mail: liuyw@nimte.ac.cn; runweili@nimte.ac.cn

The ORCID identification number(s) for the author(s) of this article can be found under https://doi.org/10.1002/aisy.202000235.

Prof. Y. Liu, Prof. J. Shang, Prof. R.-W. Li
Center of Materials Science and Optoelectronics Engineering
University of Chinese Academy of Sciences
Beijing 100049, China

Prof. Y. Liu, Prof. R.-W. Li
School of Future Technology
University of Chinese Academy of Sciences
Beijing 100049, P. R. China

Dr. Y. Wu, Y. Zhou, W. Asghar, Prof. Y. Liu, F. Li, D. Sun, C. Hu, Z. Wu, Prof. J. Shang, Z. Yu, Prof. R.-W. Li, Dr. H. Yang
Zhejiang Province Key Laboratory of Magnetic Materials and Application Technology
Ningbo Institute of Materials Technology and Engineering
Chinese Academy of Sciences
Ningbo 315201, P. R. China

ADVANCED
SCIENCE NEWS

www.advancedsciencenews.com

ADVANCED
INTELLIGENT
SYSTEMS
Open Access

www.advintellsyst.com

substrate and minimizes the problem of hysteresis. This type of behavior is absent in other conductive materials (silver, gold, carbon, etc.) because of their rigid nature.[10] However, there exists a week compatibility between LM and elastomeric substrate, which influences the final properties of the strain sensor. Therefore, it is important to improve the compatibility of LM and elastic substrate. Selective wetting and transferring process is found useful to precisely pattern LM's complex geometries and to attain improved compatibility between LM and elastomeric substrate.[9,11]

In this article, we report a LM-based stretchable resistive strain sensor, prepared by using selective wetting and transferring process to attain improved compatibility between LM and polydimethylsiloxane (PDMS) substrate. Our sensor exhibits broad strain sensing range of 105%, with ultralow detection limit (0.05%) both under normal and prestretch condition, negligible hysteresis, high mechanical robustness, fast response time (58 ms), and excellent repeatability. When capability of sensor is practically demonstrated, our sensor successfully detected various human activities, such as blink motion monitoring, voice intensity differentiation, heartbeat and wrist pulse monitoring. Moreover, strain sensor incorporated smart glove and smart kneecap are used to detect various human gestures, which confirms the potential of our sensor in the field of human–machine interaction.

2. Results and Discussion

2.1. Working Principle of Strain Sensor

The design concept of our strain sensor is based on deformability-dependent resistive sensing mechanism. The relative change in resistance ($\Delta R/R_0$) of our sensor during stretching is expressed by following equation

$$\frac{\Delta R}{R_0} = \varepsilon^2 + 2\varepsilon \tag{1}$$

where ΔR and R_0 show the respective resistances of sensor during stretched and normal states, and ε shows the strain acting on sensor. The mathematical proof of aforementioned equation is given in the Supporting Information.

2.2. Preparation Process of the Strain Sensor

Figure 1a shows the fabrication process of LM-based strain sensor in which a selective wetting and transferring approach is used to pattern LM Galinstan on PDMS substrate. This patterning approach gives high compatibility between the LM and elastomeric substrate of sensor.[12] Process starts by submerging strain gauge-shaped copper foil in NaOH solution. NaOH removes the gallium oxide layer of LM and makes it suitable for further processing. Then, Galinstan is injected on the top of copper foil by using syringe, which results in the formation of strain gauge-shaped LM film on the top of copper foil. Galinstan exhibits hydrophilic behavior toward copper and hydrophobic (repulsive) behavior toward plastic that is why Galinstan thin film is only formed on copper foil rather than on plastic supporting the copper foil (Figure S1, Supporting Information). LM film deposited copper foil is cleaned in deionized water, followed by drying it in air. Afterward, liquid PDMS is poured on copper foil, dispersed by a glass slide, and then cured at 80 °C for 30 min. After complete curing, PDMS is peeled off, which results in the transfer of strain gauge-shaped LM film from copper foil to the PDMS substrate. During peeling operation, LM and PDMS remain stick with each other due to the presence of LM oxide layer, formed during prior exposure of LM film to air. This oxide layer improves the interfacial interaction between LM and PDMS, as shown in Figure S2, Supporting Information. Finally, we deposited another layer of PDMS for packaging purpose, which completes the formation of LM-based strain sensor. Figure 1b shows the initial and stretched state of strain sensor. Figure 1c shows the high stretchability of sensor.

2.3. Electromechanical Properties of the Strain Sensor

Figure 2 shows the electromechanical properties of sensor. It is evident from Figure 2a that our sensor exhibits stable performance under repeated strains of 20%, 40%, 60%, 80%, and
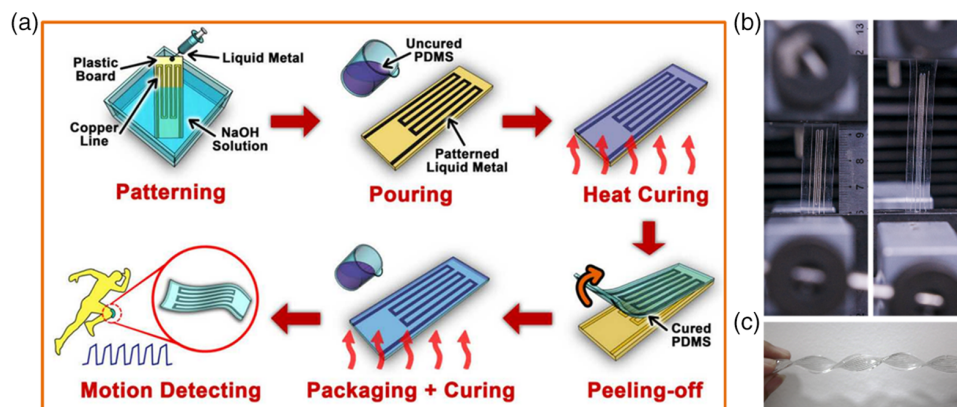

Figure 1. Fabrication of LM-embedded strain sensor. a) Schematic illustration showing the fabrication process of strain sensor. LM Galinstan is patterned on PDMS substrate by using selective wetting and transferring approach. b) Figure showing the normal and stretched state of strain sensor. c) Figure showing the high stretchability of sensor.
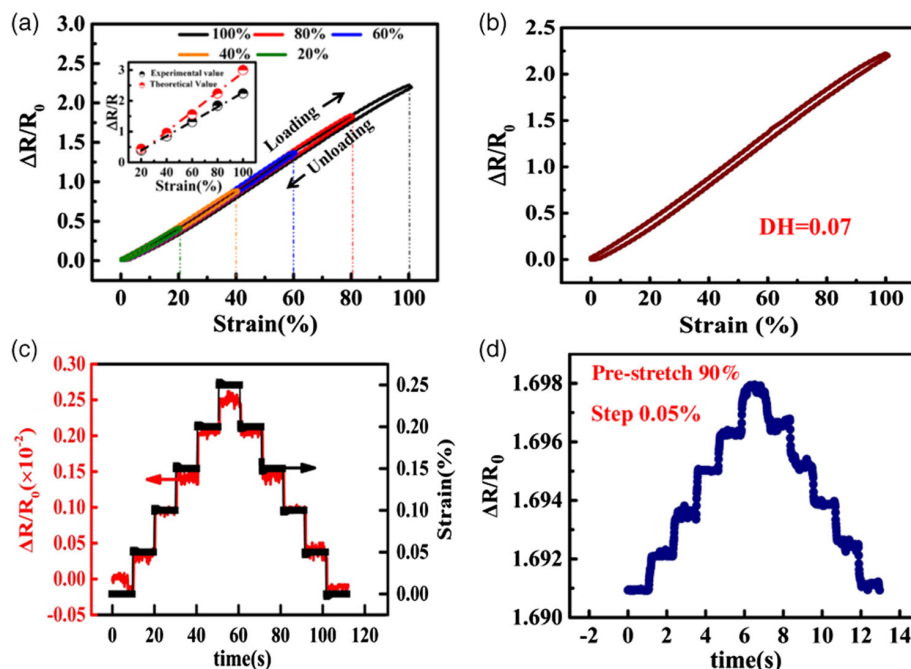
Figure 2. Electromechanical characterization of strain sensor. a) Sensor's performance under repeated strains of 20%, 40%, 60%, 80%, and 100% (rate = 100 mm min^{-1}). Sensor exhibits high gauge factor of 2.33 and linear response to applied strains. b) Relative resistance variation of sensor under 100% cyclic strain, indicating low DH. c) Sensor's response to cyclic strains under normal condition. d) Sensor's response to cyclic strain under prestretch condition (90%).

100%. Relative resistance of sensor increases with the increase in strain, which confirms the existence of linear relationship between relative resistance and applied strain. When theoretical and experimental performance of sensor is compared (inset of Figure 2a), theoretical curve slightly deviates from the experimental curve. This occurs because only uniform deformation of fluidic channel is considered in the derivation of Equation (1). Deformation of the cross-sectional area along the longitudinal direction can also occur unevenly depending on the sensor geometry. In addition, the nonuniform deformation can give rise to a different sensitivity from the aforementioned theoretical prediction. Under the strain range of 0–100%, our sensor depicted gauge factor of 2.33, which is calculated by the following formula

$$\text{GF} = \frac{\Delta R/R_0}{\varepsilon} = 2 + \varepsilon \tag{2}$$

In addition, our sensor exhibits Young's modulus of ≈1.1 MPa and typical elastomeric behavior, which is evident from the sensor's stress–strain curves (Figure S3, Supporting Information). If A shows the area under hysteresis curve then degree of hysteresis (DH) of sensor is quantified by the following equation[13]

$$\text{DH} = \frac{A_{\text{loading}} - A_{\text{unloading}}}{A_{\text{loading}}} \times 100\% \tag{3}$$

where A_{loading} and $A_{\text{unloading}}$ are the area of loading and unloading response curves, respectively. Figure 2b shows that our sensor exhibits negligible DH (0.07) even under 100% stretching

strain. Low hysteresis of sensor is attributed to the fluidic nature of LM combined with viscoelasticity of PDMS, which makes our sensor highly responsive to stretching and releasing strain. The hysteresis curves of sensor under 20% and 60% stretching strain are shown in Figure S4, Supporting Information. Figure 2c shows the dynamic response of sensor under increasing cyclic strains of 0.05%, 0.10%, 0.15%, 0.20%, and 0.25%. Our sensor exhibits stable response to increasing cyclic strain while
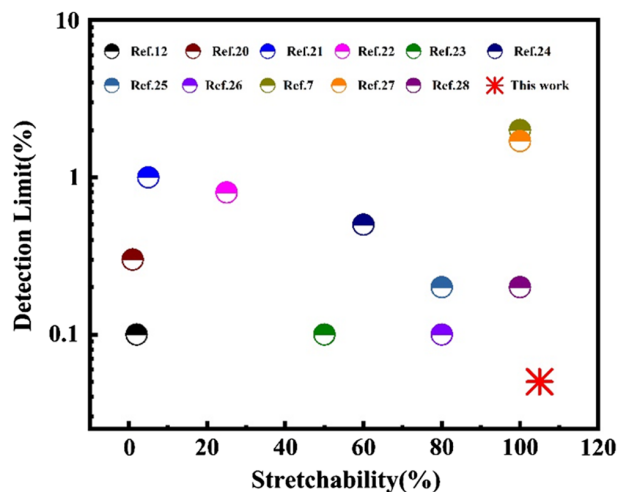

Figure 3. Detection limit comparison of current and previously reported strain sensors, as a function of their stretchability.

**ADVANCED
SCIENCE NEWS**
www.advancedsciencenews.com

**ADVANCED
INTELLIGENT
SYSTEMS**
Open Access
www.advintellsyst.com

its resistance increases regularly with the applied load. Moreover, sensor is fully capable to detect strains below 0.1%. Afterward, we prestretched our sensor to 30%, 60%, 90%, and 105% strains and again evaluated its performance under increasing cyclic strains (Figure 2d and Figure S5, Supporting Information). Impressively, our sensor again showed a stable response toward repeated strains, which confirms that current sensor exhibits high resolution and is fully capable of detecting minute and large applied strain, both in normal and prestretched condition. Excellent elasticity of PDMS combined with high conductivity of LM are the factors, responsible for ultralow detection limit of sensor. This demonstrates the potential applications of sensor in the field of human−machine interaction.

Figure 3 shows the detection limit comparison of current and previously reported strain sensors, as a function of their stretchability.[4,7,14] Figure confirms that our sensor exhibits least detection limit (0.05%) within the 0–105% strain range, when compared with previously reported strain sensors. Due to this factor, our sensor exhibits superior capability of measuring and distinguishing slight motions, even under the prestretched strain of 105%.

For various strain-sensing applications, stability, reproducibility, response time, and durability of sensor also play important role. **Figure 4**a shows the resistance variation of sensor with respect to stretching cycles. Sensor's resistance increases with the increase of stretching strain, but resistance variation remains
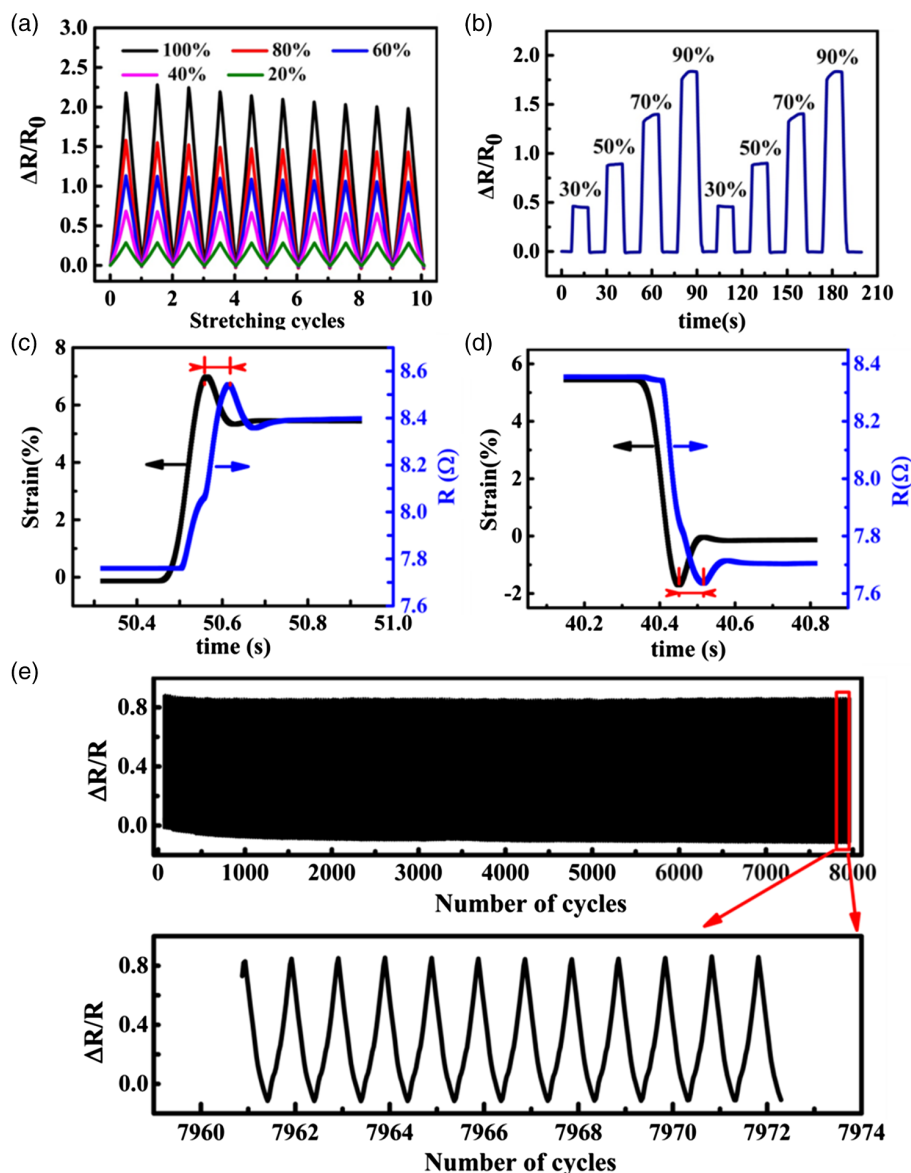

Figure 4. a) Sensor's resistance variation as a function of stretching cycles. b) Relative resistance variation under increasing cyclic strain, confirming the good repeatability of sensor. c,d) Sensor's loading and unloading response time, evaluated under 0.05% strain (rate = 2400 mm min^{-1}). Sensor exhibits a response time of (58 ± 5) ms. e) Durability of the sensor evaluated for ≈8000 cycles under 50% applied strain, showing sensor's excellent mechanical robustness. Inset shows the detailed resistance signals from 7961 to 7972 cycles.

constant during specific strain, which demonstrates the steady response of sensor. Sensor's response toward dynamic cyclic strain is shown in Figure 4b in which sensor's resistance remained constant during the holding operation. Overall, our sensor presented good repeatability within the strain range of 90%, which satisfies the requirements for human–machine interface applications.[15] To determine the sensor's response time, we applied 0.05% strain on sensor by using computer-controlled material testing machine (Instron 5943, USA) (2400 mm min^{-1}) and response time is obtained by calculating the time lag between resistance and strain curves. Sensor presents a response time of (58 ± 5) ms (Figure 4c,d), which is comparable to the response time of previously reported strain sensors.[8] In addition, our sensor endured $\approx$8000 loading–unloading cycles under 50% strain (rate $= 100$ mm min^{-1}), without showing any obvious fatigue (Figure 4e). This confirms the high mechanical robustness of our sensor. Inset of Figure 4e shows that resistance signal keeps its amplitude and waveform at different stages, confirming the high stability of the device. The superior performance of our LM strain sensor, especially in terms of wide range strain sensing (105%), ultralow detection limit (0.05%), minimal hysteresis (DH $= 0.07$), excellent mechanical robustness ($\approx$8000 cycles), and fast response time (58 ms) makes the current manufacturing method very useful, when compared with previously published literture.[16]

2.4. Application Demo of the Strain Sensor

The ultralow-detection limit, broad sensing range combined with good stretchability, greatly broadens the application of strain sensor. So, we attached our sensor on different locations of human body (such as canthus, throat, chest, and wrist) to monitor various human activities (**Figure 5**). First, the strain sensor was fixed on the canthus to see its response to the lower movements induced by blink (Figure 5a). Our sensor successfully detected the subtle motion of blink, in real time. Furthermore, the sensor was attached on human throat to detect vibration signals, produced due to speaking of different words such as "Liquid," "Metal," "Sensor," and "NIMTE" (Figure 5b). Our sensor has efficiently distinguished the various vibration signals of vocal cords produced during human speech, which demonstrate the potential applications of our sensor in the field of phonation rehabilitation exercise and human–machine interaction. In addition, the sensor was attached on the chest for heartbeat monitoring and it was clearly detected by our sensor (Figure 5c). In addition, when we attached our sensor on human wrist, it also efficiently detected the wrist pulse (as expected). (Figure 5d). The wrist pulse waves with ten peaks were recorded for 5 s, indicating a pulse rate of 120 times per minute during exercise.

We developed sensors incorporated smart glove to track the motion of each human finger. Smart glove contains a printed circuit board chip, which is connected to robotic hand via Bluetooth. We mounted a smart glove on human hand and a remotely placed robotic hand was operated from distant position, by using the various gestures of glove mounted human hand (**Figure 6**). Smart glove precisely controlled the robotic fingers, without using any additional control algorithms for grasping and releasing of objects (Movie S1, Supporting Information). This proves that current smart glove can be successfully used in virtual reality applications, to track the activities of various human body parts.
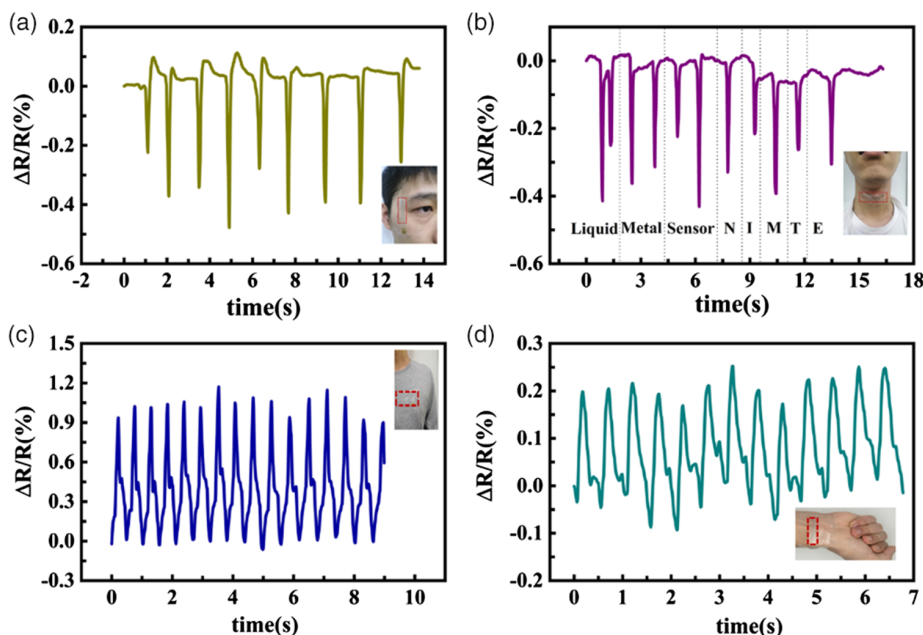

Figure 5. Application demo of our sensor for the monitoring of various human activities. a) Sensor's resistance variation caused due to subtle motion of blink. Sensor is attached on canthus. b) Resistance variation of strain sensor attached to human throat when the wearer speaks "Liquid," "Metal," "Sensor," and "NIMTE." c) Response of sensor during the human heartbeat monitoring. d) Sensor's resistance change induced by the wrist pulse during exercise.
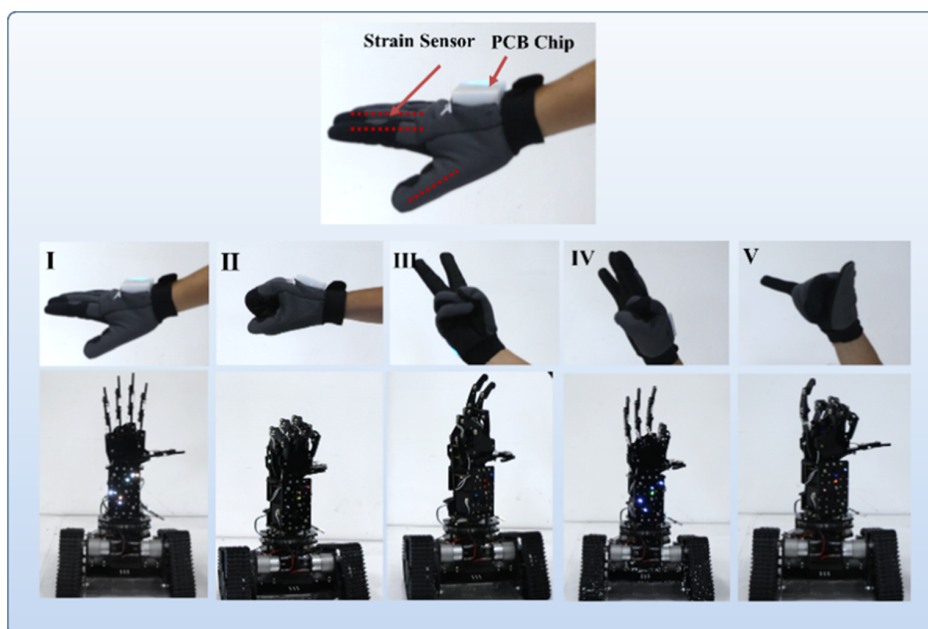
Figure 6. Application demo of strain sensor. Robotic hand operated from a remote position, by using the various gestures of glove mounted human hand.

We prepared a smart kneecap by attaching our sensor on it, and then used that smart kneecap to record knee's bending motion. During the running motion, sensor's resistance changed accordingly with the straightening and bending motion of knee (**Figure 7**). When knee returns to its original position, the resistance also returns to its baseline. More interestingly, our sensor successfully distinguished the repeated bending of knee joint, with different amplitude and frequency (Figure 7 and Movie S2, Supporting Information), which demonstrates

its great potential to be applied in the field of human–machine interaction.

Furthermore, the sensor mounted kneecap was used for the purpose of virtual reality and interactive gaming (Movie S3, Supporting Information). The movie shows the gesture-driven video game, operated due to the movement of sensor mounted kneecap. It is evident from movie that sensor successfully detects the minute signals arising from joint motion-induced skin stretch, which proves its full capability to be used in the field of virtual reality.
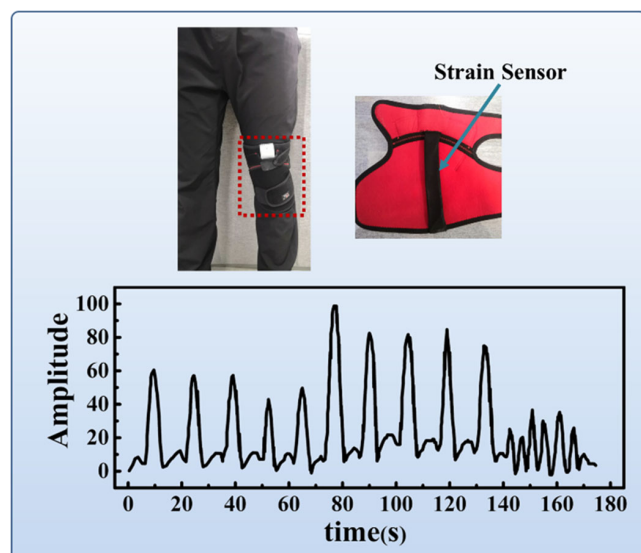
3. Conclusion

In this article, LM-based stretchable strain sensor is prepared by using selective wetting and transferring process, to get improved compatibility between LM and PDMS substrate. Our sensor exhibits broad strain sensing range (105%) with ultralow detection limit (0.05%), minimal hysteresis, high mechanical robustness ($\approx$8000 cycles), fast response time (58 ms), and excellent repeatability. Outstanding combinations of LM's high electrical conductivity with excellent elastic properties of PDMS are the factors responsible for superior behavior of our sensor. As LM exhibits fluidic nature, so it deformed similar to elastic PDMS substrate without showing any elastic mismatch, and enabled our sensor to detect minute and larger strains at the same time, with negligible hysteresis. When demonstrated practically, our sensor successfully detected various human activities, such as blink motion monitoring, voice intensity differentiation, and heartbeat and wrist pulse monitoring. Moreover, the detection of various human gestures by strain sensor illustrates the capability of sensor for effective human health and motion monitoring, virtual reality, and interactive gaming applications.

Figure 7. Sensor's real-time response to amplitude of the human knee motion. After 140 s, the frequency of signal is increased due to fast movement of human knee.

As practically demonstrated, our sensor can be utilized either as a standalone device or key component in electronic skin and smart textiles for the applications of HMI, human motion monitoring, robotics, and beyond.

4. Experimental Section

Materials and Chemicals: High purity metals gallium, indium, and tin (99.99%, Beijing Founde Star Sci. & Technol. Co., Ltd) were mixed together in the ratio of 67.3:19.2:13.5 by mass. Then, the aforementioned mixture was heated and stirred at 60 °C for 30 min to obtain LM Galinstan ($Ga_{67.3}In_{19.2}Sn_{13.5}$). Sodium hydroxide (NaOH) was purchased from Sinopharm Chemical Reagent Co., Ltd. Strain gauge-shaped copper foil and PDMS (Sylgard 184, Dow Corning, USA) were purchased from market. Cu foil was already deposited on plastic board and after cleaning, it was used without any further modification. PDMS was prepared in a 10:1 w/w ratio (base to curing agent) and then degassed to remove air bubbles.

Fabrication of Strain Sensors: Strain gauge-shaped Cu foil was cleaned and submerged in NaOH solution (250 mmol L^{-1}) and Galinstan was poured on it by using syringe. LM stuck on Cu patterns (copper patterns) due to its hydrophilic behavior toward copper. Afterward, PDMS was spin coated on the Cu patterns and cured at 70 °C for 1 h, followed by peeling it with transfer printing machine. Finally, the package layer of PDMS was deposited to complete the formation of sensor. Prior to the deposition of PDMS package layer, square-shaped flexible copper electrodes were attached with LM, which later served as electrodes. During manufacturing of sensor, deposited PDMS layers were cured in an electric oven. The final size of sensor was 3.5 cm × 1 cm × 1 mm and dimensions of patterned LM include, 3 cm length, 300 µm line width, and 30 µm thickness.

Characterization and Performance Testing: Mechanical tests were conducted by using computer-controlled material testing machine (Instron 5943, USA). Electromechanical tests were performed at room temperature by using a two-probe configuration. The electrical current was provided by current source device (Keithley 237, Keithley Instruments, USA), whereas the voltage was measured by voltmeter (Keithley 6517A, Keithley Instruments, USA).

The experiments involving human subjects have been performed with the full, informed consent of the volunteers.

Supporting Information

Supporting Information is available from the Wiley Online Library or from the author.

Conflict of Interest

The authors declare no conflict of interest.

[1] a) J. X. Wang, M. F. Lin, S. Park, P. S. Lee, *Mater. Today* **2018**, *21*, 508; b) R. Herbert, J.-H. Kim, Y. S. Kim, H. M. Lee, W.-H. Yeo, *Materials* **2018**, *11*, 187; c) H. Wang, X. Ma, Y. Hao, *Adv. Mater. Interfaces* **2017**, *4*, 1600709.

[2] a) J. A. Rogers, T. Someya, Y. Huang, *Science* **2010**, *327*, 1603; b) Y. Huang, Y. Ding, J. Bian, Y. Su, J. Zhou, Y. Duan, Z. Yin, *Nano Energy* **2017**, *40*, 432.

[3] M. Amjadi, K.-U. Kyung, I. Park, M. Sitti, *Adv. Funct. Mater.* **2016**, *26*, 1678.

[4] M. Amjadi, A. Pichitpajongkit, S. Lee, S. Ryu, I. Park, *ACS Nano* **2014**, *8*, 5154.

[5] a) G. Cai, J. Wang, K. Qian, J. Chen, S. Li, P. S. Lee, *Adv. Sci.* **2017**, *4*, 1600190; b) S. Gong, D. T. H. Lai, Y. Wang, L. W. Yap, K. J. Si, Q. Q. Shi, N. N. Jason, T. Sridhar, H. Uddin, W. L. Cheng, *ACS Appl. Mater. Interfaces* **2015**, *7*, 19700; c) O. Kanoun, C. Muller, A. Benchirouf, A. Sanli, T. N. Dinh, A. Al-Hamry, L. Bu, C. Gerlach, A. Bouhamed, *Sensors* **2014**, *14*, 10042.

[6] D. J. Lipomi, M. Vosgueritchian, B. C. K. Tee, S. L. Hellstrom, J. A. Lee, C. H. Fox, Z. Bao, *Nat. Nanotechnol.* **2011**, *6*, 788.

[7] D. Kang, P. V. Pikhitsa, Y. W. Choi, C. Lee, S. S. Shin, L. Piao, B. Park, K.-Y. Suh, T.-I. Kim, M. Choi, *Nature* **2014**, *516*, 222.

[8] L. J. Lu, Y. J. Zhou, J. Pan, T. Q. Chen, Y. J. Hu, G. Q. Zheng, K. Dai, C. T. Liu, C. Y. Shen, X. M. Sun, H. S. Peng, *ACS Appl. Mater. Interfaces* **2019**, *11*, 4345.

[9] M. D. Dickey, *Adv. Mater.* **2017**, *29*, 1606425.

[10] Y.-H. Wu, R.-M. Zhen, H.-Z. Liu, S.-Q. Liu, Z.-F. Deng, P.-P. Wang, S. Chen, L. Liu, *J. Mater. Chem. C* **2017**, *5*, 12483.

[11] a) N. Kazem, T. Hellebrekers, C. Majidi, *Adv. Mater.* **2017**, *29*, 1605985; b) C. Pan, E. J. Markvicka, M. H. Malakooti, J. Yan, L. Hu, K. Matyjaszewski, C. Majidi, *Adv. Mater.* **2019**, *31*, e1900663.

[12] Y. Jiang, S. Su, H. Peng, H. S. Kwok, X. Zhou, S. Chen, *J. Mater. Chem. C* **2017**, *5*, 12378.

[13] S. G. Yoon, H. J. Koo, S. T. Chang, *ACS Appl. Mater. Interfaces* **2015**, *7*, 27562.

[14] a) S. Chen, Y. Wei, S. Wei, Y. Lin, L. Liu, *ACS Appl. Mater. Interfaces* **2016**, *8*, 25563; b) L. Lu, X. Wei, Y. Zhang, G. Zheng, K. Dai, C. Liu, C. Shen, *J. Mater. Chem. C* **2017**, *5*, 7035; c) J. Lee, S. Kim, J. Lee, D. Yang, B. C. Park, S. Ryu, I. Park, *Nanoscale* **2014**, *6*, 11932; d) M. Amjadi, M. Turan, C. P. Clementson, M. Sitti, *ACS Appl. Mater. Interfaces* **2016**, *8*, 5618; e) Y.-H. Wu, H.-Z. Liu, S. Chen, X.-C. Dong, P.-P. Wang, S.-Q. Liu, Y. Lin, Y. Wei, L. Liu, *ACS Appl. Mater. Interfaces* **2017**, *9*, 20098; f) J. Y. Kim, S. Ji, S. Jung, B.-H. Ryu, H.-S. Kim, S. S. Lee, Y. Choi, S. Jeong, *Nanoscale* **2017**, *9*, 11035; g) Q. Liu, J. Chen, Y. Li, G. Shi, *ACS Nano* **2016**, *10*, 7901; h) E. Roh, B.-U. Hwang, D. Kim, B.-Y. Kim, N.-E. Lee, *ACS Nano* **2015**, *9*, 6252; i) Y. Cheng, R. Wang, J. Sun, L. Gao, *Adv. Mater.* **2015**, *27*, 7365.

[15] T. Yamada, Y. Hayamizu, Y. Yamamoto, Y. Yomogida, A. Izadi-Najafabadi, D. N. Futaba, K. Hata, *Nat. Nanotechnol.* **2011**, *6*, 296.

[16] a) J. Chen, J. Zhang, Z. Luo, J. Zhang, L. Li, Y. Su, X. Gao, Y. Li, W. Tang, C. Cao, Q. Liu, L. Wang, H. Li, *ACS Appl. Mater. Interfaces* **2020**, *12*, 22200; b) D. Y. Choi, M. H. Kim, Y. S. Oh, S.-H. Jung, J. H. Jung, H. J. Sung, H. W. Lee, H. M. Lee, *ACS Appl. Mater. Interfaces* **2017**, *9*, 1770; c) Y. Zhou, Y. Wu, W. Asghar, J. Ding, X. Su, S. Li, F. Li, Z. Yu, J. Shang, Y. Liu, R.-W. Li, *ACS Appl. Electron. Mater.* **2019**, *1*, 1866; d) P. Cao, Y. Liu, W. Asghar, C. Hu, F. Li, Y. Wu, Y. Li, Z. Yu, S. Li, J. Shang, X. Liu, R.-W. Li, *Adv. Eng. Mater.* **2020**, *22*, 1901239.

2000235 (8 of 8)